Integration of Vehicle Dynamic Model and System Identification Model for Extending the Navigation Service Under Sensor Failures

Penggao Yan, Weisong Wen, *Member, IEEE*, and Li-Ta Hsu, *Senior Member, IEEE*

***Abstract*—Accurate and reliable localization is of great importance for autonomous vehicles (AV). Mainstream localization approaches in autonomous vehicles (AV) are limited by the reliability of onboard sensors, which could be vulnerable to sensor failure, such as signal outages of the camera and signal spoofing of the global navigation satellite systems (GNSS). Different from these active or passive sensors, the vehicle dynamic model (VDM), which is the application of physical laws to a vehicle in motion, is environmentally independent and is capable of providing vehicle motion estimation continuously. However, the performance of the VDM-based motion estimation is dominated by the accuracy of the system dynamics model. To tackle this issue, this study proposes a sensor-free localization method VDM-SI by integrating system identification into the design of vehicle dynamic models (VDM). A system identification process based on low-order process models is proposed to identify the system dynamics of the AV, where the identified system responses are taken as the control input of VDM to estimate the vehicular positioning. The localization experiments in two scenarios show that the mean absolute translation error of VDM-SI can be reduced by 70% compared to conventional VDM methods. In addition, VDM-SI is experimentally proven to improve the localization performance of sensor fusion-based localization systems with high noise levels. Furthermore, in the application of re-localization after sensors fail and recover, VDM-SI shows strength in enhancing the security of AVs in extreme conditions.**

***Index Terms*—Autonomous vehicles, localization, sensor failure, system identification, vehicle dynamic models.**

I. INTRODUCTION

Automated Driving Systems (ADS) and their carrier, autonomous vehicles (AV), have received increasing and close attention from academia and industry [1], [2]. Among the four basic components of AVs, including localization, perception, planning, and control module [3], [4], localization plays a fundamental role in providing essential information for the successful execution of other modules. Specifically, accurate localization can roughly define and reduce the searching space of perception tasks [5] and provide the initial constraint for the planning module to generate feasible trajectories [6], [7]. More importantly, localization plays a vital role in generating collision-free trajectories, which ensures safe navigation [8]. Research works on the localization of AV can be mainly divided into two categories based on the utilized sensors, including active or passive sensors-based localization and environmentally independent VDM-based localization. The former relied on the quality of the measurements collected by sensors affected by the environments. The latter is environmentally independent but relies on the modeling of the system dynamics.

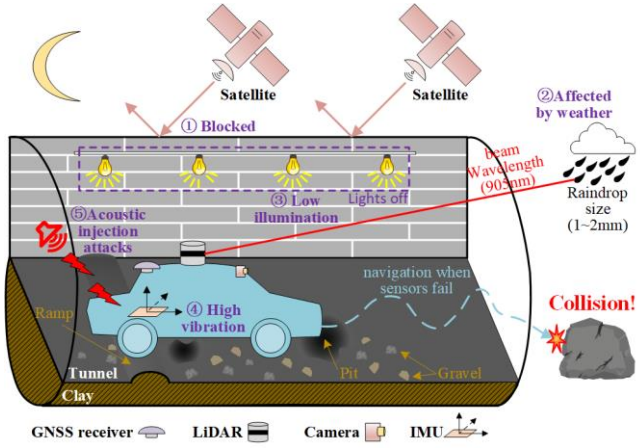

Fig. 1. A scenario where the GNSS receiver, LiDAR, camera, and IMU may fail simultaneously. GNSS signals are blocked when the AV is running in a tunnel. LiDAR detection is affected by raindrops. The performance of cameras degrades under low illumination. The vehicle is running on a gravel road with some pits, where IMU may fail in such highly vibrating conditions. Acoustic injection attacks will cause malfunctions in IMU. The AV produces inaccurate localization results with sensor failures, facing a high risk to collide.

Active or passive sensors-based localization methods: In mainstream localization solutions in AVs, sensor-based approaches are dominant and can provide reliable localization results in most scenarios. Global navigation satellite system (GNSS) receivers [9], light detection and ranging (LiDAR) [10], cameras [11], and inertial measurement units (IMU) [12] are the most commonly used sensors in these solutions. However, there still exists extreme cases that human drivers can easily handle, but AVs are unable to manage due to the inherent limitations of these sensors [13]. Fig. 1 shows a scenario where the GNSS receiver, LiDAR, camera, and IMU may fail simultaneously. GNSS receivers cannot receive

This work was supported by funded by the Guangdong Basic and Applied Basic Research Foundation (2021A1515110771) and University Grants Committee of Hong Kong under the scheme Research Impact Fund (R5009-21). This research was also supported by the Faculty of Engineering, The Hong Kong Polytechnic University under the project "Perception-based GNSS PPP-RTK/LVINS integrated navigation system for unmanned autonomous systems operating in urban canyons".

The authors are with the Department of Aeronautical and Aviation Engineering, Hong Kong Polytechnic University, Hong Kong (e-mail: penggao.yan@connect.polyu.hk; welson.wen@polyu.edu.hk; lt.hsu@polyu.edu.hk).

GNSS signals in an underground environment, such as tunnels and sewage canals [14], since GNSS signals will be blocked by physical. In addition, GNSS signals can also be spoofed by manipulating the signals, such as retransmitting captured GNSS signals after a delay [15], [16]. In GNSS-denied situations, LiDAR or camera sensors are usually adopted to capture environment features to eventually obtain localization solutions [17]. However, LiDAR detector is vulnerable to adverse weather conditions such as rain, snowing, and fogging. The wavelength of LiDAR in most autonomous driving systems usually has three types, including 905 nm, 940 nm, and 1550 nm [18], while the raindrop size is significantly larger, usually ranging from 1mm to 2mm, which means that raindrops can be detected by LiDAR. Therefore, the ability of LiDAR detectors will degrade on rainy days since raindrops will be detected as objects, disturbing the detection of landmarks, vehicles, and other objects of interest [19], [20]. The performance of camera sensors is also affected by the environment, especially by lighting conditions. Specifically, the performance of the visual feature detection and tracking would be significantly degraded due to extremely low and unstable illumination conditions [21]. When a LiDAR or camera produces excessive errors, IMU is usually adopted to provide localization in a short period. In the localization community, IMU has been regarded as a robust solution and has been integrated into various localization and navigation systems for a long time [22], [23]. However, IMU may fail in some extreme conditions, such as highly vibrating environments [24]. In addition, Micro-electro-mechanical systems (MEMS) inertial sensors are known to be spoofed by acoustic injection attacks, which exhibit extra forces on the sensing mass of the MEMS accelerometers [25]. A number of flight crashes have been attributed to IMU failure, such as the crashes of Adam Air 574 [26]. Although countermeasures are developed, such as using multiple IMUs to increase the system redundancy [27], conducting IMU failure detection aided by other sensors [28], and even utilizing deep learning technologies to predict the increment of the vehicle position during sensor failures [29], these approaches still make an underline assumption that at least one sensor for localization functions well. However, human drivers can deal with those complexities with experience and common sense. Although researchers have been developing advanced algorithms to improve the performance of these sensor-based localization approaches, it is not enough to produce the desired localization performance unless the development of these sensors can overcome their inner limitations and become robust to spoofing signals. Therefore, instead of purely being enabled by sensors, it is worthwhile to investigate the possibility of utilizing information from other sources to improve localization performance and fight for sensor failures.

Environmentally independent VDM-based localization: One possible way is to re-examine vehicle dynamic models (VDMs) since localization methods based on them are not affected by sensors' conditions. According to the definition of the Society of Automotive Engineers (SAE), vehicle dynamic model is the application of physical laws to a vehicle in motion [30]. Scientifically speaking, an accurate VDM can perfectly estimate the motion of the system based on the given system control inputs. Many researchers have integrated vehicle dynamics into the development of localization methods, such as the IMU/VDM integrated navigation system [28], [31] and the motion compensation in constructing accurate LiDAR observations for localization tasks [32]. However, vehicle dynamic models applied in these methods usually make some assumptions about the environments and simplification of the system complexity which may overlook the latency (the time required to reach a steady response) caused by control systems [33]. As AVs usually operate in a changing and highly unpredictable environment, vehicle dynamic models can hardly consider all influencing factors and guarantee a good localization result when sensors fail. Nevertheless, vehicle dynamic models have been widely applied in AVs for multiple tasks, such as the update process in the extended Kalman filter (EKF) based localization method [34] and Ackerman turning geometry in turning control [35]. In these applications, vehicle dynamic models provide a coarse estimation of the system state while corrections on it are made by sensors' measurements in different perspectives to generate a reliable estimation eventually. For example, measurements about vehicle position from exogenous sensors will correct the estimation made by vehicle dynamic models in the EKF-based localization process. Unfortunately, such kind of corrections is still limited by potential sensor failures. Fortunately, system identification brings the opportunity to provide a new kind of correction to VDM when AVs encounter sensor failures. System identification is a term in the control field that refers to the technology of "building mathematical models of dynamic systems from observed input-output data"[36]. As the estimation errors of VDM mainly come from unknown system characteristics and changing environments, it is tough to consider all these factors in modeling VDM with specialized knowledge, such as the cornering stiffness of tires and the bank angle of roads [37]. However, the knowledge of system identification can be applied to estimate the system responses affected by these factors in a data-driven approach [38], consequently correcting VDM estimation by providing a better control input signal than raw control commands.

In light of this finding, this study aims to bridge the gap between vehicle dynamic models and system identification to provide a reliable ego-localization for AVs when sensors fail in a short period. In particular, this paper proposes a sensor-free localization method VDM-SI by integrating the system identification into the design of VDM. Specifically, essential system dynamics of the AV are first identified by utilizing perception, planning, and control information when sensors function well. Then the identified system dynamics is used to estimate the system response of the AV, which is integrated into the control input design of VDM to provide reliable ego-localization under sensor failures. In addition, the proposed VDM-SI is integrated with noisy sensor information from LiDAR matching with prior maps via an extended Kalman filter (EKF) [39] to demonstrate the ability of VDM-SI in improving the localization performance of mainstream localization systems. The contributions of this study are as there folds:

(1) A universal sensor-free localization method. This study

proposes a sensor-free localization method by integrating system identification into the design of vehicle dynamic models when AVs have sensor failures, enhancing the resilience of AVs in extreme conditions. In particular, the proposed method is not limited to a specific vehicle dynamic model but is applicable to all kinds of vehicle dynamic models.

(2) Extendable to fusion-based localization system. This study experimentally demonstrates the proposed method can be easily integrated into mainstream sensor fusion-based localization systems, improving their localization performance under significantly high noise levels.

(3) Bridge the gap between control and localization. This study builds the bridge between system identification of the control system and localization in the autonomous system, which demonstrates the potential of endogenous information in autonomous systems to enhance its ability on localization tasks, and encourages researchers to explore this direction.

The structure of the paper is as follows. The first section reviews the limitation of sensor-based localization in autonomous vehicles and briefly introduces the proposed sensor-free localization method, whose overall architecture is illustrated in Section II. Section III describes the VDM-based localization method and discusses its limitation from a mathematical view. Section IV first introduces the basic process of system identification and proposes the VDM-SI method by integrating VDM and system identification. In Section V, an extended Kalman filter is constructed by fusing the proposed VDM-SI and noisy sensors. Numerical experiments are conducted in Section VI to evaluate the system identification performance and the localization performance of the proposed method. In addition, the ability of VDM-SI to enhance the security of AVs in extreme conditions is examined in a re-localization and resuming navigation experiment. Finally, the last section presents a summary.

II. Overview of the Proposed Integration System

As discussed in Section I, all sensors have inevitable limitations and cannot guarantee stability and correctness under certain circumstances. However, nearly all navigation solutions in AVs heavily rely on sensors. As AVs have been gradually becoming an important part of human society, it might be fatal even if all sensors fail in a short period. Therefore, a sensor-free localization method is needed to extend the navigation service under sensor failures, serving as a 'life-saving mechanism' before sensors recover.

The architecture of the proposed method is shown in Fig. 2. When AVs operate normally with well-functioning sensors, an offline system identification process is executed to identify the system dynamics of two plants in AVs, including the powertrain and the steering system. Control commands obtained from planning and control modules are regarded as the input data of system identification. At the same time, the responses of plants, such as linear velocity and angular velocity measured by sensors, are taken as the output data. When AVs have sensor failures, the identified system dynamics is utilized to estimate the system response of control commands, which is taken as the control input of the VDM to estimate the ego-pose of the vehicle. Such pose estimation could be used to develop an advanced localization system based on sensor fusion methods, such as Kalman filters [40] and factor graph optimization [41]. To ease the reading, we list all used symbols in Table IX in the appendix.

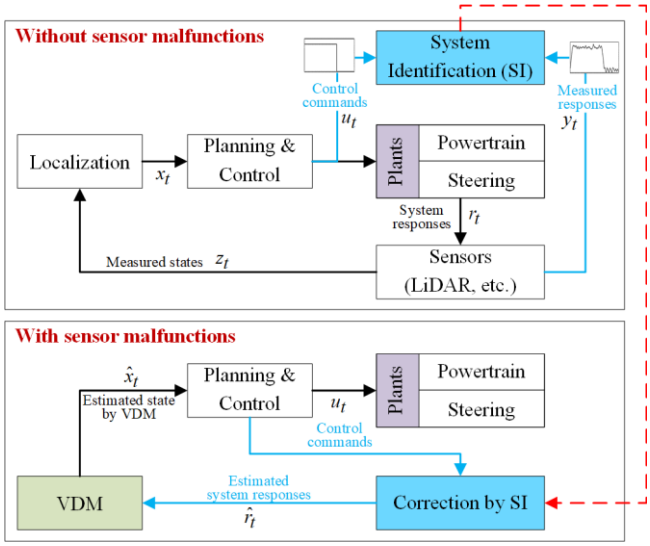

Fig. 2. The architecture of the proposed method.

III. Vehicle Dynamic Models Based Localization

Vehicle dynamic model (VDM) is the application of physical laws to a vehicle in motion [30], which can provide a coarse estimation of the motion of the system and is widely adopted in the development of advanced localization methods. In this study, the bicycle kinematic model [37] is employed to describe the vehicle motion and estimate the ego-pose of the vehicle based only on geometric relationships, which are not affected by sensors' conditions.

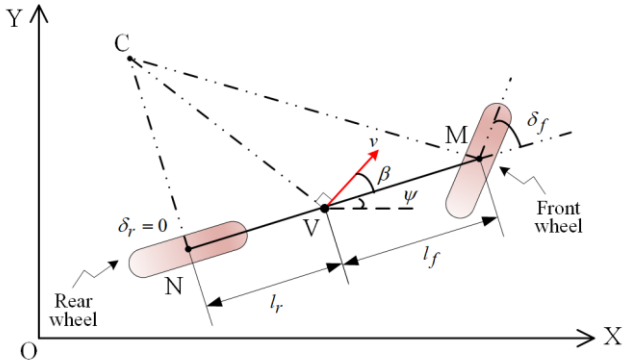

Fig. 3. The kinematic bicycle model.

A. The two-wheel bicycle kinematic model

Fig. 3. depicts the kinematic bicycle model used in this study. The left and right front wheels of four-wheel autonomous vehicles are represented by one front wheel at point M, while the two rear wheels are represented by one rear wheel at point N. Point V represents the center of gravity, dividing the wheelbase of the vehicle into two parts l_r and l_f. As mainstream autonomous vehicles adopt the front-wheel

steering mechanism, the steering angle of the front wheel is represented by δ_f while the steering angle of the rear wheel (δ_r) is set to zero. By drawing two lines perpendicular to the orientation of the front wheel and rear wheel respectively, an intersection point C is obtained, which is the instantaneous rolling center for the vehicle. In addition, the length of the line CV is the radius R of the vehicle's path and the vehicle velocity v is perpendicular to this line. With the assumption that the vehicle only moves in a plane and that slip angles at both wheels are zero under low-speed conditions [37], the slip angle of the vehicle β is defined by the direction of v with respect to the longitudinal axis of the vehicle. By applying sine rule to triangle CVM, we have:

$$\frac{\sin(\delta_f - \beta)}{l_f} = \frac{\sin\left(\frac{\pi}{2} - \delta_f\right)}{R}. \quad (1)$$

As $\delta_r = 0$, in the orthogonal triangle CVN, we have:

$$\sin(\beta) = \frac{l_r}{R}. \quad (2)$$

The slip angle β can be solved with (1) and (2):

$$\beta = \tan^{-1}\left(\frac{l_r}{l_f + l_r}\tan(\delta_f)\right). \quad (3)$$

The heading angle (ψ) of the vehicle is the angle made by the line MN and the horizontal direction. With the low-speed assumption, the rate of change of ψ is identical to the angular velocity:

$$\dot{\psi} = \frac{v}{R}. \quad (4)$$

By substituting (2) into (4), (4) can be re-written as:

$$\dot{\psi} = \frac{v}{l_r}\sin(\beta). \quad (5)$$

Then the rate of change of the horizontal movement $\dot{x}$ and the vertical movement $\dot{y}$ are given by:

$$\dot{x} = vcos(\psi + \beta), \quad (6)$$

$$\dot{y} = vsin(\psi + \beta). \quad (7)$$

Let a be the acceleration along the velocity orientation, the rate of change of velocity $\dot{v}$ is given by:

$$\dot{v} = a. \quad (8)$$

Then the planar motion of the vehicle can be described by three coordinates (x, y, ψ) using (3)(5)(6)(7)(8), where the steering angle of the front wheel δ_f and the acceleration along the velocity orientation a are the control inputs.

B. Limitations of VDM-based localization methods

Through the modeling process of the two-wheel bicycle kinematic model, one could easily observe that assumptions about wheel slip angles (the angle made by the tire axis and the wheel direction) and low-speed conditions have been made. Once these assumptions are not satisfied in the field test, localization errors arise. This phenomenon is not unique to the two-wheel bicycle kinematic model but widely exists in various vehicle dynamic models. For example, in the 14-DOF vehicle model [42], the sprung mass pitch angle and the sprung mass roll angle are assumed to be small values. In general, VDMs usually make assumptions about environments and simplification on the system's complexity. As AVs usually operate in changing and highly unpredictable environments, VDMs can hardly consider all influencing factors and guarantee a good motion estimation when sensors fail.

Furthermore, localization errors raised from the VDMs will accumulate when sensors fail to provide corrections. To quantify the localization error with time in an intuitive way, we assume the process in the planning and control module can be simplified by a linear difference equation:

$$\mathbf{u}_t = \mathbf{D}_v(\mathbf{s}_{t-1} - \mathbf{g}_t), \quad (9)$$

whereas $\mathbf{s}_{t-1}$ is the system state at time $t-1$, $\mathbf{g}_t$ is the planning goal for time instant t, $\mathbf{u}_t$ is the control command produced by the planning and control module at time t, and $\mathbf{D}_v$ is the coefficient matrix. Similarly, the vehicle motion can also be represented by a linear difference equation:

$$\mathbf{s}_t = \mathbf{A}_v\mathbf{s}_{t-1} + \mathbf{B}_v\mathbf{u}_t, \quad (10)$$

where $\mathbf{A}_v$ and $\mathbf{B}_v$ are coefficient matrices.

Assuming the estimated state by VDM at time $t-1$ is $\hat{\mathbf{s}}_{t-1}$, the control command generated in the planning and control module according to $\hat{\mathbf{s}}_{t-1}$and $\mathbf{g}_t$ can be represented by:

$$\hat{\mathbf{u}}_t = \mathbf{D}_v(\hat{\mathbf{s}}_{t-1} - \mathbf{g}_t). \quad (11)$$

For simplification, the vehicle motion depicted by VDM is written by (12), with an additional error term $\mathbf{C}_v$ compared to (10):

$$\hat{\mathbf{s}}_t = \mathbf{A}_v\hat{\mathbf{s}}_{t-1} + \mathbf{B}_v\hat{\mathbf{u}}_t + \mathbf{C}_v, \quad (12)$$

Therefore, the localization error $\mathbf{e}_t$ can be derived by the following equations:

$$\mathbf{e}_t = \mathbf{s}_t - \hat{\mathbf{s}}_t. \quad (13)$$

By substituting (10) and (12) into (13), we can obtain the recursive equation of $\mathbf{e}_t$ as below:

$$\mathbf{e}_t = \mathbf{s}_t - \hat{\mathbf{s}}_t = \mathbf{A}_v\mathbf{e}_{t-1} + \mathbf{B}_v\mathbf{D}_v\mathbf{e}_{t-1} - \mathbf{C}_v. \quad (14)$$

Then, the relationship between $\mathbf{e}_t$ and $\mathbf{e}_0$ can be derived:

$$\mathbf{e}_t = (\mathbf{A}_v + \mathbf{B}_v\mathbf{D}_v)^t\mathbf{e}_0 - \sum_{k=1}^{t}(\mathbf{A}_v + \mathbf{B}_v\mathbf{D}_v)^{k-1}\mathbf{C}_v. \quad (15)$$

As the localization error at the time t_0 is $\mathbf{e}_0 = 0$, the localization error at time t can be obtained:

$$\mathbf{e}_t = -\sum_{k=1}^{t}(\mathbf{A}_v + \mathbf{B}_v\mathbf{D}_v)^{k-1}\mathbf{C}_v = \begin{cases} -t\mathbf{C}_v & ,\mathbf{A}_v + \mathbf{B}_v\mathbf{D}_v = \mathbf{I} \\ \dfrac{(\mathbf{A}_v + \mathbf{B}_v\mathbf{D}_v)^t - \mathbf{I}}{\mathbf{A}_v + \mathbf{B}_v\mathbf{D}_v - \mathbf{I}}\mathbf{C}_v & ,\mathbf{A}_v + \mathbf{B}_v\mathbf{D}_v \neq \mathbf{I}. \end{cases} \quad (16)$$

Note that the localization error produced by VDM increases exponentially over time (except in the case $\mathbf{A}_v + \mathbf{B}_v\mathbf{D}_v = \mathbf{I}$, where the error increases linearly), whereas the error term $\mathbf{C}_v$ between VDM and real vehicle motion process plays a role as a gain factor. Due to the fact that sensors fail to provide correction to VDM estimation, the accumulated error is inevitable. However, the gain factor $\mathbf{C}_v$ can be reduced by developing advanced VDMs with higher precision. The essence is to consider system characteristics and environmental information as much as possible, such as the cornering stiffness of tires and the bank angle of roads [37]. Nonetheless, as AVs usually operate in a changing and highly unpredictable environment, vehicle dynamic models can hardly consider all influencing factors and guarantee a good localization result when sensors fail. However, these factors will affect the system performance, which can be captured by some endogenous features of the system, such as the system responses to given control commands. Through examining these endogenous features of the system, information about the unknown system characteristics and the environment change could be derived in some aspect, eventually providing

corrections to VDM-based localization systems. Inspired by this, this paper examines the endogenous feature of the system by system identification and integrates it into the VDM-based localization system, which will be illustrated in the next section.

IV. Integration of System Identification and Vehicle Dynamic Models

In most VDMs, the control inputs should be the measured physical states, such as the front wheel steering angle δ_f and the acceleration a involved in (5)-(7). When sensors fail, such measurement will be unavailable, and the control command produced by the planning and control module would be the promising alternative. In other words, VDM assumes that the system response to the control command is identical to the control command. However, the response in physical systems is different. For example, the response of a typical second-order system to a unit step input is shown in Fig. 4. The amplitude of the response gradually converges to a final state value with oscillations. In addition, the response exhibits a noticeable time delay with respect to the input signal. These phenomena also exist in a higher-order system, such as the powertrain and steering system in AVs. Note that the characteristic of the response to the input signal is related to both system characteristics and environmental conditions. For example, changing the load of a proportional integral derivative (PID) [43] controlled full direct current (DC) motor will affect its angular velocity response [44]. As AVs usually operate in a highly changing environment, the system response to the same control command may vary significantly over different time periods. Therefore, the system response can be viewed as a measurement of system states under changing environments when sensors fail. In light of this, this section will examine and model the system response of AVs' plants, including the powertrain system and the steering system, so-called system identification, which will be used to correct the estimation by the VDM-based localization system.

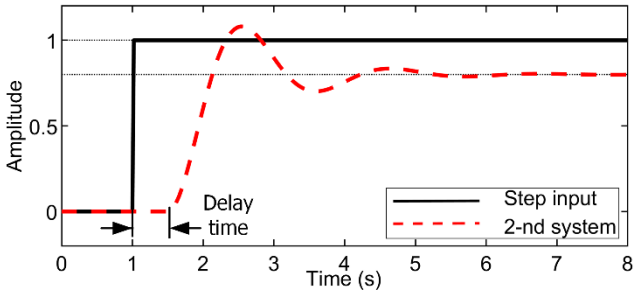

Fig. 4. The step response of a typical second-order system.

A. Introduction of system identification

To model the system response of a physical system, system identification is applied in this study. System identification is the science of "building mathematical models of dynamic systems from observed input–output data"[36]. System identification mainly consists of three procedures [38]. First, collecting the input-output data during a designed diverse experiment to ensure that data become maximally informative. Then, selecting a set of candidate models based on prior knowledge about the system or experience. In this step, models developed based on physical interpretations with adjustable parameters are so-called grey-box models, while models whose parameters lack physical meanings are called black-box models [38]. In the third step, optimizing parameters of each candidate model with the collected data and deciding the best model according to certain criterias, such as mean-square error on predicting the system dynamics.

In this study, pseudo-random binary sequence (PRBS) is used as the input signal to excite the system. PRBS is commonly used in system identification since it is the deterministic approximation of white noise in discrete time, which means that it can excite all frequencies equally well. A set of process models are chosen for the identification of the powertrain system and the steering system in AVs. In industrial practice, identification for control is usually based on the construction of low-order process models [45]. For example, the form of a typical first-order-plus-dead-time (FOPDT) process model can be denoted as follows,

$$G_{FOPDT}(s) = \frac{K_p}{1+sT_w} e^{-sT_d}, \tag{17}$$

where s is the complex frequency domain parameter, K_p is the static gain, T_w is the time constant, and T_d is the time delay. A typical second-order-plus-dead-time (SOPDT) process model can be written as below,

$$G_{SOPDT}(s) = \frac{K_p(1+sT_z)}{1+2s\zeta T_w + s^2T_w^2} e^{-sT_d}, \tag{18}$$

where T_z is the parameter related to the process zero, and ζ is the damping coefficient. A typical third-order-plus-dead-time (TOPDT) process model is given below,

$$G_{TOPDT}(s) = \frac{K_p(1+sT_z)}{(1+2s\zeta T_w + s^2T_w^2)(1+sT_{p3})} e^{-sT_d}, \tag{19}$$

where T_{p3} is related to the additional pole in the TOPDT. For more types of structures for process models, one can refer to [46]. In addition, a disturbance model based on the ARMA model is introduced to model the noise in the system. The prediction by the identified model can be formulated as below:

$$\hat{r}(s) = Gu(s) + He^w(s), \tag{20}$$

$$H = \frac{c_0 + c_1 s + c_2 s^2 + \cdots c_n s^n}{d_0 + d_1 s + d_2 s^2 + \cdots d_n s^n}, \tag{21}$$

where $u(s)$ is the input, $e^w(s)$ is the white noise, $\hat{r}(s)$ is the estimated system response in the s-domain, G is the process model, and H is the disturbance model, represented by a transfer function whose nominator and denominator are polynomials for an autoregressive moving average (ARMA) model [47]. All the above parameters will be estimated by least square optimization methods, which are commonly used in system identification [38].

To evaluate the performance of the models' parameters estimation using the least square optimization methods, three criteria including Akaike's Information Criterion (AIC) [48], fit ratio (FIT) [38], and mean-square error (MSE) are employed. Specifically, FIT measures how close the estimated model approximates the true model,

$$FIT = \left(1 - \frac{\sqrt{\sum_{t=1}^{N} {e_t^r}^2}}{\sqrt{\sum_{t=1}^{N} {}^c y_t^{r\,2}}}\right) * 100\%, \quad (22)$$

MSE focuses on the error between the model prediction and the system output,

$$MSE = \frac{1}{N}\sum_{t=1}^{N} {e_t^r}^2, \quad (23)$$

and the AIC criteria penalize MSE and the model complexity simultaneously,

$$AIC = N\log\left(\det\left(\frac{1}{N}\mathbf{e}^{s^T}\mathbf{e}^s\right)\right) + 2n_p + N\left(\log(2\pi)n_y + 1\right), \quad (24)$$

where $e_t^r = y_t^r - \hat{r}_t$, $\mathbf{e}^s = [e_1^r, e_2^r, \dots, e_N^r]^T$, ${}^c y_t^r = y_t^r - \frac{1}{N}\sum_{t=1}^{N} y_t^r$, y_t^r is the measured system response in the time domain, $\hat{r}_t$ is the estimated system response in the time domain, n_p is the number of free parameters in the model, n_y is the number of model outputs, and N is the number of samples in the estimation dataset.

B. Integrating system identification and VDM

The process model is constructed in s-domain, which cannot be directly used to predict the time response of a given input signal in the time domain. However, the control command in AVs is inherently given in the time domain. To represent the identified model in the time domain, we transfer the process model to a state-space form [49] as:

$$\dot{\mathbf{s}}^m = \mathbf{A}_s\mathbf{s}^m + \mathbf{B}_s\mathbf{u}^s + \mathbf{K}_s\mathbf{e}^\eta, \quad (25)$$

$$\mathbf{r}^o = \mathbf{C}_s\mathbf{s}^m + \mathbf{D}_s\mathbf{u}^s + \mathbf{e}^\eta, \quad (26)$$

where $\mathbf{A}_s, \mathbf{B}_s, \mathbf{C}_s, \mathbf{D}_s, \mathbf{K}_s$ are state-space parameters, $\mathbf{s}^m$ is the vector of middle states in the time-domain, $\dot{\mathbf{s}}^m$ is the derivative of $\mathbf{s}^m$ with respect to time, $\mathbf{r}^o$ is the output vector related to the estimated system response, $\mathbf{u}^s$ is the input vector related to the input commands, and $\mathbf{e}^\eta$ is the white noise vector. The value of $\mathbf{A}_s, \mathbf{B}_s, \mathbf{C}_s, \mathbf{D}_s, \mathbf{K}_s$ can be derived by using the method described in [49].

Therefore, the estimated system responses can be applied to VDM models under sensor failures, as shown in Fig. 2. In this study, we mainly identify the powertrain system and the steering system in AVs. Assuming the estimated system response of the powertrain system to the acceleration command is $\hat{a}$, and the estimated system response of the steering system to the steering command is $\hat{\delta}_f$, VDM will adopt $\hat{a}$ and $\hat{\delta}_f$ as the control inputs. The modified VDM is named **VDM-SI**, which can be represented below:

$$\dot{x} = v\cos(\psi + \beta), \quad (27)$$

$$\dot{y} = v\sin(\psi + \beta), \quad (28)$$

$$\dot{\psi} = \frac{v}{l_r}\sin(\beta), \quad (29)$$

$$\dot{v} = \hat{a}, \quad (30)$$

$$\beta = \tan^{-1}\left(\frac{l_r}{l_f + l_r}\tan(\hat{\delta}_f)\right). \quad (31)$$

V. Fusion with Noisy Sensors Based on Extended Kalman Filters

In localization systems, sensor measurements are usually coupled with noises that might be too large to produce reliable localization results. To tackle this issue, fusion methods, such as Kalman filters (KF), are employed to fuse the information from multi-source sensors and motion models. More specifically, the KF-based fusion method consists of two components: the measurement equation based on sensor measurements; and the state equation based on motion models. When sensor measurements are largely affected by noises, the localization performance will highly rely on the prediction accuracy arising from the motion model. To explore the ability of VDM-SI in improving the localization performance of these fusion methods with noisy sensor measurements, this section integrates VDM-SI with LiDAR in a loosely coupled structure based on the extended Kalman filters (EKF) [39]. In particular, the NDT-matching algorithm [50], which is a typical matching algorithm for the LiDAR matching problem, is deployed to estimate the ego-pose of the vehicle based on raw LiDAR point clouds, and the VDM-SI is used to construct the propagation function. The performance of the fusion system will be discussed in Section VI-D.

A. Discretization and Linearization

The differential equations of VDM-SI in (27)-(31) need to be integrated into differences equations to account for discrete time intervals. Assuming the velocity of the vehicle is constant during a short period Δt, we have:

$$x_{k+1} = x_k + v_k\cos(\psi_k + \beta_{k+1})\Delta t, \quad (32)$$

$$y_{k+1} = y_k + v_k\sin(\psi_k + \beta_{k+1})\Delta t, \quad (33)$$

$$\psi_{k+1} = \psi_k + \frac{v_k}{l_r}\sin(\beta_{k+1})\Delta t. \quad (34)$$

By assuming the acceleration is also constant during Δt, we have:

$$v_{k+1} = v_k + \hat{a}_{k+1}\Delta t. \quad (35)$$

Besides, the discrete form of (31) is given below:

$$\beta_{k+1} = \tan^{-1}\left(\frac{l_r}{l_f + l_r}\tan(\hat{\delta}_{f,k+1})\right). \quad (36)$$

Define $\mathbf{s}_k = [x_k, y_k, \psi_k, v_k]^T$ as the state vector of the vehicle at time instant k, the above equations could be represented with a non-linear function $f(\cdot)$ as:

$$\mathbf{s}_{k+1} = f(\mathbf{s}_k, \hat{a}_{k+1}, \hat{\delta}_{f,k+1}). \quad (37)$$

By taking the first-order Taylor expansion at point $(\hat{x}_k, \hat{y}_k, \hat{\psi}_k, \hat{v}_k)$, the Jacobian matrix of $f(\cdot)$ can be obtained as below:

$$\mathbf{F}_k = \left.\frac{\partial f(\mathbf{s}_k, \hat{a}_{k+1}, \hat{\delta}_{f,k+1})}{\partial \mathbf{s}_k}\right|_{\mathbf{s}_k = [\hat{x}_k, \hat{y}_k, \hat{\psi}_k, \hat{v}_k]^T}$$

$$= \begin{bmatrix} 1 & 0 & -\hat{v}_k\sin(\hat{\psi}_k + \beta_{k+1})\Delta t & \hat{v}_k\cos(\hat{\psi}_k + \beta_{k+1})\Delta t \\ 0 & 1 & \hat{v}_k\cos(\hat{\psi}_k + \beta_{k+1})\Delta t & \hat{v}_k\sin(\hat{\psi}_k + \beta_{k+1})\Delta t \\ 0 & 0 & 1 & \frac{\sin(\beta_{k+1})}{l_r}\Delta t \\ 0 & 0 & 0 & 1 \end{bmatrix}, \quad (38)$$

B. Fusion based on Extended Kalman Filter

By introducing the process noise $\mathbf{w}_k$ which is assumed to be a zero-mean Gaussian noise with covariance $\mathbf{Q}_k = diag(\delta_p^2, \delta_p^2, \delta_\psi^2, \delta_v^2)$, where δ_p, δ_ψ and δ_v are the standard deviation of the position component, the orientation component, and the velocity component in the process noise, respectively. The state equation in (37) could be written as:

$$\mathbf{s}_{k+1} = f(\mathbf{s}_k, \hat{a}_{k+1}, \hat{\delta}_{f,k+1}) + \mathbf{w}_k. \quad (39)$$

Define $\mathbf{z}_k$ as the estimated pose by the NDT-matching algorithm [50], and $\boldsymbol{\eta}_k$ as the measurement noise which is assumed to be a zero-mean Gaussian noise with covariance $\mathbf{R}_k = diag(\sigma_p^2, \sigma_p^2, \sigma_\psi^2)$, where σ_p and σ_ψ are the standard deviation of the position component and the orientation component in the measurement noise, respectively. The measurement function could be written as:

$$\mathbf{z}_k = \mathbf{M}_k \mathbf{s}_k + \boldsymbol{\eta}_k, \tag{41}$$

$$\mathbf{M}_k = \begin{bmatrix} 1 & 0 & 0 & 0 \\ 0 & 1 & 0 & 0 \\ 0 & 0 & 1 & 0 \end{bmatrix}. \tag{42}$$

Based on (39) and (40), the fusion of VDM-SI and LiDAR measurement can be achieved by a general extended Kalman filter [39]. For clarity, the integrated system is denoted as EKF-VDM-SI.

VI. Numerical Experiments

A. Setup of the experiment platform

In this paper, all experiments are conducted in a half-simulated environment, which is created by the 3D simulator, Gazebo [51]. The main reasons for only conducting the simulation to validate the effectiveness of the proposed method are listed below:

(1) This paper aims to explore the potential of VDM during sensor failures. Since the dynamic model cannot be perfectly recovered for the real AV system, by utilizing the simulation, the parameters of the system dynamic model can be adjusted and labeled easily.

(2) The control and path planning would affect the performance of the VDM. Therefore, it is hard to exclude impacts of the AV system control and planning on the VDM-based localization. Compared to a field study, it is much easier to control variables and set up experiments in a simulated environment [52], [53].

(3) The recently developed simulators for the AV are quite mature to simulate the dynamics and raw sensor measurements, such as Gazebo [51] and CARLA [54], which inspired us the perform the validation using the simulated dataset.

In the experiment, an autonomous vehicle with full autonomy is employed as the experiment platform, whose software stack is developed based on Autoware [4], an open-source autonomous driving software. Specifically, a Velodyne HDL-32 LiDAR is adopted to measure the vehicle states, including position, orientation, velocity, and acceleration, providing essential information for the development of the localization module, which mainly adopts the NDT-Matching algorithm [50]. The planning module is mainly based on the A-star algorithm [55], while the control module simply employs the pure pursuit algorithm [56]. As the main research focuses on localization performance, an obstacle-free environment is assumed, indicating that the localization module can provide essential information for the AV to move from the start point to the endpoint. Therefore, we omit the construction of the perception module to highlight the main point. The typical parameters of the vehicle model in Gazebo are listed in Table I. In this chapter, all the computations are conducted using a desktop (Intel Core i7-10700 CPU, 2.90 GHz).

TABLE I
TYPICAL PARAMETERS OF THE VEHICLE MODEL IN GAZEBO

Parameters	Wheel radius	Wheel width	Wheel-base	Wheel tread	Vehicle length
Value	0.34 m	0.23 m	2.95 m	1.55 m	4.82 m
Parameters	Vehicle width	Vehicle height	Minimum turning radius	Maximum steering angle	
Value	1.81 m	1.5 m	2.95°	97.3°	

B. Performance of system identification

In the simulated vehicle by Gazebo, two plants including the powertrain and the steering system are employed. The powertrain consists of the engine and all of the components that convert the engine's power into the movement of the vehicle, including transmission, driveshafts, differential, and axles [57]. The steering system consists of the steering wheel, the steering column, the steering gear, and other necessary components that turn the vehicle around the vertical axis while driving [58]. In the Autoware-Gazebo simulation, the powertrain system is designed to receive the velocity command from the control module and then drive the vehicle to move, while the steering system is designed to receive the steering angle command to turn the front wheels.

1) **Identification of the Powertrain System:** In the identification of the powertrain system, a PRBS last for 60 seconds is adopted as the velocity command to stimulate the powertrain. The sampling rate of the PRBS is set to 100 Hz, and its amplitude is set to 1 m/s, as shown in Fig. 5. The output data for the system identification is the real velocity of the AV measured by LiDAR and IMU. The steering command is kept to zero during the experiment. The collected input-output data is split into two parts: the first 30-seconds part with 3000 samples is used for estimation, and another 30-seconds part is for validation. Then a set of candidate models based on the low-order process model with delay and addictive ARAM disturbance model is constructed, where the order of poles range from 1 to 3, the order of zeros ranges from 0 to 1, and the order of disturbance model ranges from 0 to 2. Table II lists the structure of these candidate models.

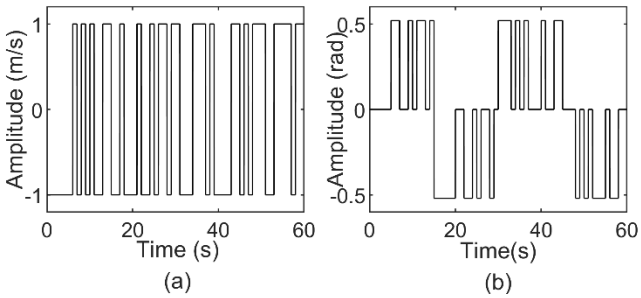

Fig. 5. Input signals for identifying (a) the powertrain system; (b) the steering system.

TABLE II
THE STRUCTURE OF CANDIDATE MODELS

Candidate models	Order of poles	Order of zeros	Order of disturbance model
Px	1, 2, 3	0	0
PxZ	1, 2, 3	1	0
PxD	1, 2, 3	0	0
PxDZ	1, 2, 3	1	0
PxEy	1, 2, 3	0	1, 2

PxZEy	1, 2, 3	1	1, 2
PxDEy	1, 2, 3	0	1, 2
PxDZEy	1, 2, 3	1	1, 2

Note: 'P' represents poles, 'Z' represents zeros, 'D' represents time delay, 'E' represents the disturbance model, 'x' represents the order of poles, and 'y' represents the order of disturbance model.

By employing least square optimization, the optimal parameters of each model are estimated. Table III shows the performance of these models on the estimation and validation dataset. As can be seen, P3DZE2 and P3DE2 have the same lowest AIC on the estimation dataset, while the former significantly outperforms the latter in terms of FIT and MSE on the validation dataset, suggesting that P3DZE2 (the TOPDT with one zero and a second-order ARMA disturbance model) is the best model among the candidate set. We notice that P3DZ has a competitive performance on FIT and MSE, but its AIC is considerably lower than that of P3DZE2. The only difference between P3DZE2 and P3DZ is the existence of the second-order ARMA disturbance model, whose effects are explored by conducting residual analysis, as shown in Fig. 6.

TABLE III
PERFORMANCE OF CANDIDATE MODELS IN IDENTIFYING THE POWERTRAIN SYSTEM

Candidate Models	Evaluation on Estimation Dataset	Evaluation on Validation Dataset	
	AIC	FIT	MSE
P3DZE2	**-1.03E+01**	**80.39%**	**9.00E-03**
P3DZ	-4.45E+00	**80.03%**	**9.33E-03**
P2DZ	-3.95E+00	74.56%	1.52E-02
P3DE2	-1.03E+01	73.02%	1.70E-02
P3DZE1	-9.40E+00	70.67%	2.01E-02

Note: only the top five models with the highest FIT on the validation dataset are presented.

The autocorrelation of output residual for P3DZ is almost outside the 99% confidence interval, suggesting that most part of the residual could have been predicted from past data. Furthermore, the large magnitude of the cross correlation for P3DZ indicates that the residual is significantly influenced by specific inputs, demonstrating the deficiency of P3DZ in modeling the system dynamics. In contrast, P3DZE2 significantly performs better both on the autocorrelation analysis and the cross-correlation analysis. The additional disturbance model in P3DZE2 improves the modeling ability of the process model in identifying the powertrain. Therefore, P3DZE2 is chosen as the best model in the candidate set. Since the kinematic bicycle model takes acceleration as the control input, the time derivative of the identified velocity response is applied to obtain the acceleration response.

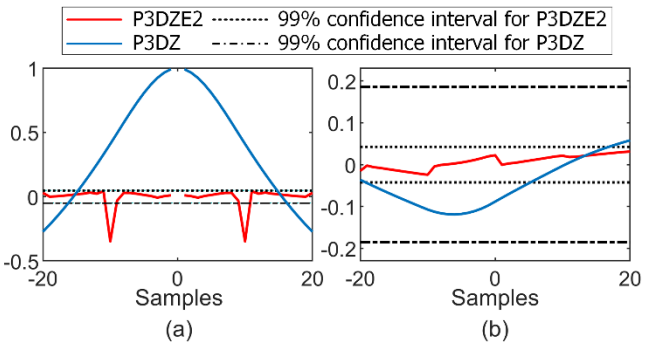

Fig. 6. Residual analysis of candidate models in identifying the powertrain system: (a) autocorrelation of residuals for output; (b) cross correlation for input and output residuals.

2) **Identification of the Steering System**: The process of identificating the steering system is similar to that of the powertrain. A PRBS with an amplitude of 0.52 rad (around 30 degrees) is adopted as the steering angle command to stimulate the steering system. LiDAR measures the angular velocity of the vehicle, which is converted to the steering angle by applying the Ackermann steering geometry [37]. The calculated steering angle is taken as the output data in the identification process. In addition, the velocity of the vehicle is set to 1 m/s during the whole process.

As shown in Table IV, P2ZE2 has the lowest AIC among the candidate, while its FIT is marginally lower than P3DZU. Furthermore, residual analysis in Fig. 7 indicates that P2ZE2 is more applicable than P3DZ. This finding is consistent with the result in the identification of the powertrain system, suggesting that the process model with a disturbance model can better approximate the steering system. It is interesting to find that the order of well-performed candidate models in the powertrain system identification is relatively higher than that in the steering system identification, possibly indicating that the powertrain system is more complex than the steering system. The identified models are then transferred to a state-space form, which will be used to estimate the acceleration response and the steering response in the time domain.

TABLE IV
PERFORMANCE OF CANDIDATE MODELS IN IDENTIFYING THE STEERING SYSTEM

Candidate Models	Evaluation on Estimation Dataset	Evaluation on Validation Dataset	
	AIC	FIT	MSE
P3DZ	-6.75E+00	**85.61%**	**5.11E-04**
P2ZE2	**-1.23E+01**	**85.18%**	**5.42E-04**
P2D	-6.65E+00	85.14%	5.45E-04
P2E2	-1.23E+01	85.05%	5.51E-04
P3ZE2	-1.23E+01	82.90%	7.21E-04

Note: only the top five models with the highest FIT on the validation dataset are presented.

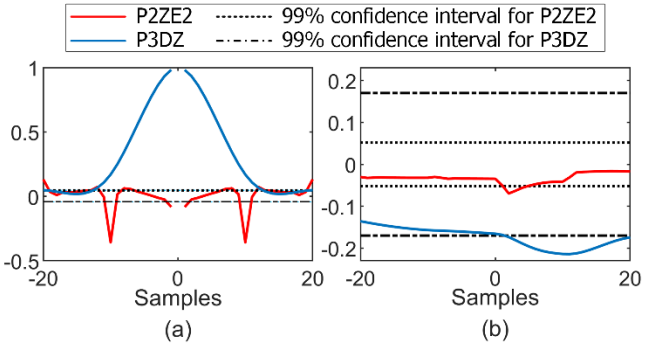

Fig. 7. Residual analysis of candidate models in identifying the steering system: (a) autocorrelation of residuals for output; (b) cross-correlation for input and output residuals.

C. Localization performance of VDM-SI

In this section, the localization performance of VDM and VDM-SI are compared in two scenarios, as shown in Fig. 8.

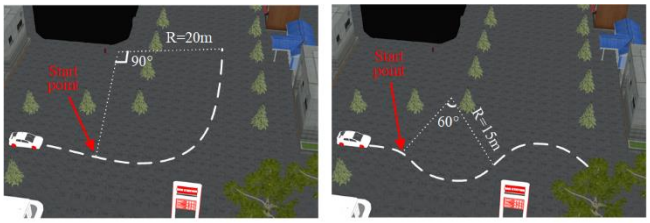

Fig. 8. Test scenarios. (a) a 90-degree bend with radius of curvature equal to 20m; (b) a S-Curve with radius of curvature equal to 15m. The white dash line is the designed track.

1) **Performance along a 90-Degree Bend**: In the first scenario, the autonomous vehicle is required to move along a 90-degree bend with a radius of curvature equal to 20 m at a constant speed of 30 km/h. LiDAR and IMU measurements provide essential information to the localization module of AV, keeping the vehicle running on the track. VDM and VDM-SI are implemented in a separate program to estimate the vehicle pose, which is only used for comparison.

Fig. 9a shows the translation error of the localization results by VDM and VDM-SI. As can be seen, the translation error of VDM increases faster than that of VDM-SI. For a quantitative comparison, the absolute translation error (ATE) of VDM and VDM-SI along the 90-degree bend are calculated and listed in Table V. The mean ATE of VDM-SI decreases by more than 70% compared to that of VDM, while a similar result is found in the max ATE and the rmse ATE, indicating that VDM-SI could effectively improve the localization performance.

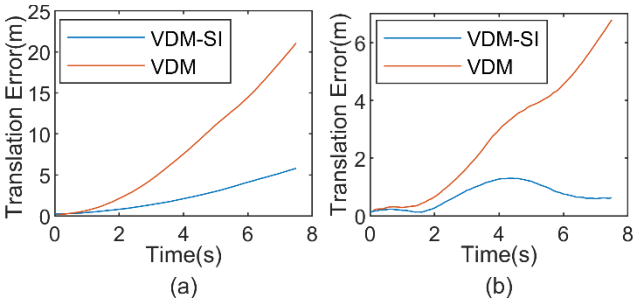

Fig. 9. The translation error of localization results of VDM-SI and VDM along (a) the 90-degree bend and (b) the S-Curve.

TABLE V
THE LOCALIZATION PERFORMANCE OF VDM AND VDM-SI IN THE TWO TEST SCENARIOS

Scenario	ATE (m)	VDM [37]	VDM-SI	Improved by VDM-SI
90-degree bend	MAX	21.65	5.87	72.88%
	MEAN	8.27	**2.44**	**70.44%**
	RMSE	10.53	2.94	72.07%
S-Curve	MAX	8.35	1.30	84.37%
	MEAN	3.20	**0.70**	**78.05%**
	RMSE	4.03	0.80	80.26%

Note: The VDM is the benchmark method in this experiment and is specifically refers to the kinematic bicycle model [37] in this paper.

2) **Performance along a Roundabout**: In the second scenario, the AV is required to move along an S-curve with a radius of curvature equal to 15 m at a constant speed of 15 km/h. Similar to the experiment steps in the first scenario, the localization performance of VDM and VDM-SI along the S-curve is evaluated. As shown in Fig. 9b, the translation error of the localization results by VDM-SI is consistently smaller than that of VDM. Table V presents the ATE of each method along the S-Curve. It is shown that VDM-SI has around 78% lower mean ATE than VDM, which is consistent with the result in the 90-degree bend experiment.

D. Localization performance of EKF-VDM-SI with noisy sensors

In this section, the localization performance of EKF-VDM-SI is examined with noisy sensor measurements at different noise levels. The autonomous vehicle is required to trace a pre-designed track at a constant speed of 5 km/h, as shown in Fig. 10. Similar to the setting of Section VI-C, the localization module utilizes LiDAR to produce accurate localization results, enabling the normal operation of the planning and control modules, thus keeping the vehicle stick tightly to the track. The EKF-VDM-SI is implemented in a separate program to estimate the ego-pose of the vehicle, where its measurements are the pose estimation results by the NDT-matching algorithm based on a simulated LiDAR sensor [50]. The prediction frequency of the EKF is set to 100 Hz, and the frequency of LiDAR measurements is set to 10 Hz. To change the noise level of the simulated LiDAR sensor, we added zero-mean Gaussian noises with different standard deviations to the raw LiDAR measurements. For comparison, EKF-VDM also is constructed by integrating VDM and the same measurements. In both EKF-VDM-SI and EKF-VDM, the initial pose is given by the estimated pose from NDT-matching, the initial position error is set to 2 m, the initial orientation error is set to 0.5 rad, and the initial velocity error is set to 1 m/s. The covariance matrix of the process noise is set to be $\mathbf{Q}_k = diag(0.2^2, 0.2^2, 0.1^2, 0.4^2)$. The covariance matrix of the measurement noise R_k is set according to the noise level of the simulated LiDAR sensor.

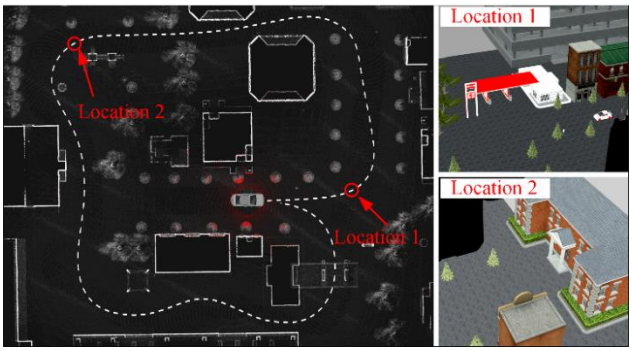

Fig. 10. The simulated environment created by Gazebo. The designed track is marked with a white dash line. The locations on the track where sensors start to fail are pointed out by red arrows.

Fig. 11 plots the trajectory of the estimated pose by EKF-VDM-SI under different noisy levels of measurements. The trajectories of the estimated pose by NDT-matching and the ground truth pose are also plotted for visualization. As can be seen, with the increase of the noise level, the estimated pose by NDT-matching gradually loses the ability to reflect the actual state of the vehicle. Nevertheless, EKF-VDM-SI demonstrates good localization performance in all cases. Table VI shows the mean absolute translation error (ATE) of the localization results by EKF-VDM-SI and EKF-VDM in each

noisy level. When the standard deviation of the added noise is 2 meters, both methods can estimate the pose accurately. Nonetheless, the mean ATE of EKF-VDM-SI is more than 17% smaller than that of EKF-VDM. With the increase of the noise level, the superiority of EKF-VDM-SI over EKF-VDM is maintained and becomes more apparent. Specifically, when the standard deviation of the added noise is 4 meters and 6 meters, EKF-VDM-SI has around a 28% reduction in mean ATE compared to EFK-VDM. Interestingly, this advantage of EKF-VDM-SI is reduced with the standard deviation of the added noise increased to 8 meters. The improvement by EKF-VDM-SI on mean ATE is reduced to around 18% in such a case. One possible reason is that the measurement noise is too large to guarantee the performance of EKF-based localization methods, which limits the improvement brought by VDM-SI.

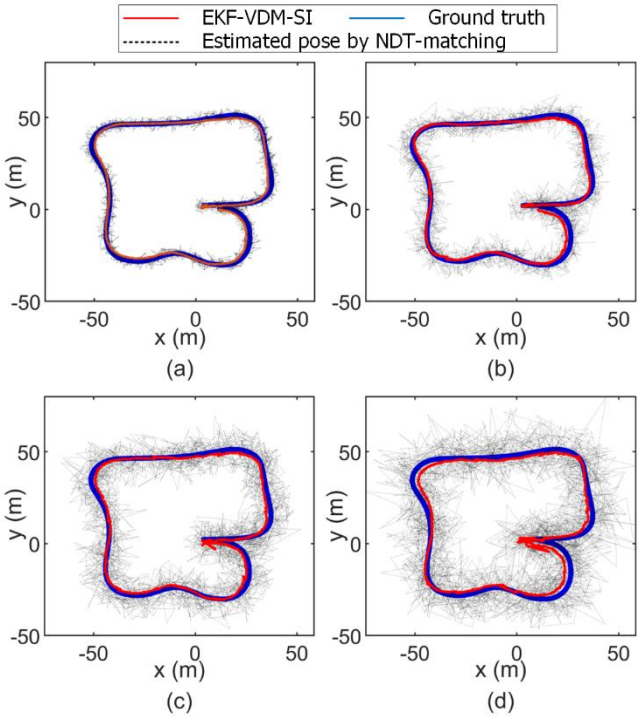

Fig. 11. The trajectory of the estimated pose by EKF-VDM-SI with noisy LiDAR measurements. Zero-mean gaussian noise is added into raw LiDAR measurements with the standard deviation of (a) 2m; (b) 4m; (c) 6m; (d) 8m.

TABLE VI
THE LOCALIZATION PERFORMANCE OF EKF-VDM AND EKF-VDM-SI UNDER DIFFERENT SENSOR NOISE LEVELS

Std. of the added noise (m)	EKF-VDM	EKF-VDM-SI	Improved by VDM-SI
2	1.15	0.95	17.45%
4	2.01	1.44	**28.29%**
6	2.30	1.66	**27.62%**
8	2.81	2.30	18.20%

TABLE VII
THE COMPUTATIONAL TIME OF THE SUBPROCESSES IN THE EKF-VDM-SI (MILLISECOND: MS)

Items	System Identification	State prediction	Measurement update	Total
MEAN (ms)	0.05	0.13	0.24	0.20
STD (ms)	0.02	0.04	0.06	0.09
Max (ms)	0.21	0.35	0.46	0.59

The computational time of system identification as well as other subprocesses in the EKF-VDM-SI are listed in Table VII. As can be seen, the mean computation time of system identification is only 0.05 ms, while the value of the state prediction process and the measurement update process in EKF are 0.13 ms and 0.24 ms, respectively. Therefore, the additional computation burden introduced by system identification is relatively small. Furthermore, the mean and maximum total computation time of EKF-VDM-SI are 0.20 ms and 0.59 ms, respectively, which are less than 10 ms. Since the prediction frequency of the EKF is 100 Hz (i.e., the maximum allowable computation time for each solution is 10 ms), EKF-VDM-SI ensures a real-time localization solution.

E. Application on re-localization with sensor failures

This section focuses on a real-world application of the proposed method: re-localization and resuming navigation after sensors fail and recover. It is possible for an AV to have sensor failures for a short time, during which the AV cannot localize itself precisely. Before sensors recover, the AV might not stop immediately and would move to an arbitrary location. At the moment that sensors recover, the AV has to re-localize itself to resume the navigation, where a good guess of the current position would be beneficial and even dominates the re-localization result. The reason is simple: a good initial guess can reduce the search efforts when the re-localization algorithms match the measured feature with the database. In this experiment, the initial guess will be provided by VDM or VDM-SI.

TABLE VIII
THE ACCOMPLISHMENT OF THE RE-LOCALIZATION AND RESUMING NAVIGATION TASK AFTER SENSORS FAIL AND RECOVER BASED ON THE INITIAL GUESS BY VDM AND VDM-SI

Outage Time (s)	Sensors Fail at location 1		Sensors Fail at location 2	
	VDM	VDM-SI	VDM	VDM-SI
3	**Success**	**Success**	**Success**	**Success**
3.5	Fail	**Success**	**Success**	**Success**
4	Fail	Fail	**Success**	**Success**
5	Fail	Fail	**Success**	**Success**
6	Fail	Fail	Fail	**Success**
7	Fail	Fail	Fail	**Success**
8	Fail	Fail	Fail	Fail

In a simulated environment created by Gazebo, as shown in Fig. 10, we start the autonomous vehicle with a well-functioning LiDAR. The AV would track a pre-designed trajectory at a constant velocity of 5 km/h. At the same time, the localization module adopts the NDT-Matching algorithm to estimate the ego-pose of the vehicle based on the LiDAR measurements. Note that LiDAR is the only source to capture environment information and obtain localization solutions in this experiment. Since the focus of this experiment is to evaluate the ability of VDM-SI to enhance the security of AVs with sensor failures, we do not utilize multiple sensors to construct a complicated localization system. After the AV arrives at the specified location, the LiDAR is shut down, and the AV purely relies on VDM or VDM-SI for localization and navigation. After Δt seconds (the outage time), the LiDAR is recovered, and the localization module starts to re-localize the vehicle. In this experiment, the concern is whether the navigation task is resumed successfully. As shown in Fig. 10,

we randomly selected two locations on the track for the experiment.

The accomplishment of the re-localization task is shown in Table VIII. At location 1, VDM and VDM-SI can ensure the success of re-localization under the outage time of fewer than 3 seconds. However, the VDM method fails to promise success in re-localization with an increased outage time. In contrast, the VDM-SI can still handle the task even though the outage time increased to 3.5 seconds. At location 2, the VDM-SI can even ensure success in re-localization under a outage time of 7 seconds. However, the VDM fails the task even when the outage time is 6 seconds. Since the NDT-Matching algorithm is sensitive to the initial conditions [59], the improved performance of VDM-SI on re-localization and resuming navigation indicates that VDM-SI could provide a more accurate initial guess of position than VDM.

VII. Conclusion and Future Work

This study proposes a sensor-free localization method by integrating system identification into the design of vehicle dynamic models, providing reliable localization results when AVs have sensor failures. When sensors function well, a system identification process is conducted to model the system dynamics of the powertrain system and the steering system. When sensors fail, the identified system dynamics is utilized to estimate the response of control commands, which is taken as the control input of VDM.

The localization results under two scenarios demonstrate that introducing system identification can significantly improve the localization performance of VDMs, where the mean absolute translation error of VDM-SI is reduced by 70% compared to conventional VDM methods. In addition, we integrate VDM-SI with noisy sensors via extended Kalman filters and experimentally show that VDM-SI can improve the localization performance of mainstream fusion-based localization methods under significantly high noise levels. Furthermore, in a real-world problem, re-localization and resuming navigation after sensors fail and recover, VDM-SI shows the potential to provide a more accurate initial guess than conventional VDMs for re-localization when sensors start to recover, ensuring a higher probability of successfully resuming navigation and thus enhancing the security of AVs in extreme conditions.

This study has several limitations, which also point out future research directions. In this study, the system identification process is conducted in an offline approach, which is vulnerable to capture the system dynamics in continuously changing environments. Future research should establish an online system identification process during the normal operation of the vehicle. In addition, this study gives little concern to the mechanism of how system identification could improve localization performance. Future research could establish the causality relationship between the property of the identified system dynamics and the improvement in localization performance.

Appendix

TABLE IX

Description of Symbols.

Sym	Description	Sym	Description
Symbols in kinematic bicycle models			
δ_f	Front wheel steering angle	ψ	Orientation
δ_r	Rear wheel steering angle	(x, y)	Plane coordinates
l_f	First part of wheelbase	v	Velocity
l_r	Second part of wheelbase	a	Acceleration along the velocity direction
β	Slip angle		
Symbols in error propagation in VDM			
$\mathbf{g}_t$	Planning goal at t	$\hat{\mathbf{u}}_t$	Control commands based on the estimated state
$\mathbf{s}_t$	System state vector at t		
$\hat{\mathbf{s}}_t$	Estimated system state vector at t	$\mathbf{A}_v, \mathbf{B}_v$	The coefficient matrices in a general vehicle motion
$\mathbf{e}_t$	Localization error of general VDMs at t	$\mathbf{D}_v$	The coefficient matrix in a general control process
$\mathbf{u}_t$	Control commands based on the real state	$\mathbf{C}_v$	The additional error term
Symbols in process models			
s	The complex frequency domain parameter	ζ	The damping coefficients
		T_d	The time delay
$u(s)$	Input commands in s-domain	K_p	The static gain
		T_{p3}	The additional pole
$\hat{r}(s)$	Estimated response in s-domain	G	The transfer function of the process model
$e^w(s)$	White noise in s-domain	H	The transfer function of the disturbance model
T_w	The time constant		
T_z	The process zero		
Symbols in evaluation of identified models			
y_t^r	Measured response at t	n_p	Number of free parameters
$\hat{r}_t$	Estimated response at t	n_y	Number of model output
r_t	System response at t	N	Number of samples
Symbols in the state-space model			
$\mathbf{s}^m$	State vector	$\mathbf{A}_s, \mathbf{B}_s,$	Coefficient matrices in the
$\mathbf{u}^s$	Input vector related to control commands	$\mathbf{C}_s, \mathbf{D}_s,$ $\mathbf{K}_s$	state-space model
$\mathbf{r}^o$	Output vector related to estimated system responses	$\hat{a}$	Identified acceleration response in time-domain
$\mathbf{e}^\eta$	White noise vector	$\hat{\delta}_f$	Identified steering angle response in time-domain
Symbols in the extended Kalman filters			
Δt	Sampling time	$\mathbf{z}_t$	The estimated pose by the NDT-matching algorithm at t
$f(\cdot)$	Non-linear state function		
$\mathbf{F}_t$	Jacobian matrix of $f(\cdot)$ at t		
$\mathbf{w}_t$	Process noise at t	$\mathbf{M}_t$	Coefficient matrix in the measurement function at t
$\mathbf{Q}_t$	Covariance matrix of $\mathbf{w}_t$		
$\boldsymbol{\eta}_t$	Measurement noise at t	$\mathbf{R}_t$	Covariance matrix of $\boldsymbol{\eta}_t$

Note: "Sym" is the abbreviation of "Symbol".

References

[1] C.-Y. Chan, 'Advancements, prospects, and impacts of automated driving systems', *International Journal of Transportation Science and Technology*, vol. 6, no. 3, pp. 208–216, Sep. 2017, doi: 10.1016/j.ijtst.2017.07.008.

[2] N. Sousa, A. Almeida, J. Coutinho-Rodrigues, and E. Natividade-Jesus, 'Dawn of autonomous vehicles: review and challenges ahead', *Proceedings of the Institution of Civil Engineers - Municipal Engineer*, vol. 171, no. 1, pp. 3–14, Mar. 2018, doi: 10.1680/jmuen.16.00063.

[3] J. Wei, J. M. Snider, J. Kim, J. M. Dolan, R. Rajkumar, and B. Litkouhi, 'Towards a viable autonomous driving research platform', in *2013 IEEE Intelligent Vehicles Symposium (IV)*, Jun. 2013, pp. 763–770. doi: 10.1109/IVS.2013.6629559.

[4] S. Kato, E. Takeuchi, Y. Ishiguro, Y. Ninomiya, K. Takeda, and T. Hamada, 'An Open Approach to Autonomous Vehicles', *IEEE Micro*, vol. 35, no. 6, pp. 60–68, Nov. 2015, doi: 10.1109/MM.2015.133.

[5] K. Yoneda, A. Kuramoto, N. Suganuma, T. Asaka, M. Aldibaja, and R. Yanase, 'Robust Traffic Light and Arrow Detection Using Digital Map with Spatial Prior Information for Automated Driving', *Sensors*, vol. 20, no. 4, p. 1181, Feb. 2020, doi: 10.3390/s20041181.

[6] L. Claussmann, M. Revilloud, D. Gruyer, and S. Glaser, 'A Review of Motion Planning for Highway Autonomous Driving', *IEEE Trans. Intell. Transp. Syst.*, vol. 21, no. 5, pp. 1826–1848, May 2020, doi: 10.1109/TITS.2019.2913998.

[7] D. Gonzalez, J. Perez, V. Milanes, and F. Nashashibi, 'A Review of Motion Planning Techniques for Automated Vehicles', *IEEE Trans. Intell. Transp. Syst.*, vol. 17, no. 4, pp. 1135–1145, Apr. 2016, doi: 10.1109/TITS.2015.2498841.

[8] A. Artunedo, J. Villagra, J. Godoy, and M. D. del Castillo, 'Motion Planning Approach Considering Localization Uncertainty', *IEEE Trans. Veh. Technol.*, vol. 69, no. 6, pp. 5983–5994, Jun. 2020, doi: 10.1109/TVT.2020.2985546.

[9] J. Bressler, P. Reisdorf, M. Obst, and G. Wanielik, 'GNSS positioning in non-line-of-sight context—A survey', in *2016 IEEE 19th International Conference on Intelligent Transportation Systems (ITSC)*, Rio de Janeiro, Brazil: IEEE, Nov. 2016, pp. 1147–1154. doi: 10.1109/ITSC.2016.7795701.

[10] A. Poulose, M. Baek, and D. S. Han, 'Point Cloud Map Generation and Localization for Autonomous Vehicles Using 3D Lidar Scans', in *2022 27th Asia Pacific Conference on Communications (APCC)*, Jeju Island, Korea, Republic of: IEEE, Oct. 2022, pp. 336–341. doi: 10.1109/APCC55198.2022.9943630.

[11] N. Piasco, 'A survey on Visual-Based Localization: On the benefit of heterogeneous data', *Pattern Recognition*, p. 20, 2018.

[12] A. Ndjeng Ndjeng, D. Gruyer, S. Glaser, and A. Lambert, 'Low cost IMU–Odometer–GPS ego localization for unusual maneuvers', *Information Fusion*, vol. 12, no. 4, pp. 264–274, Oct. 2011, doi: 10.1016/j.inffus.2010.06.006.

[13] J. Vargas, S. Alsweiss, O. Toker, R. Razdan, and J. Santos, 'An Overview of Autonomous Vehicles Sensors and Their Vulnerability to Weather Conditions', *Sensors*, vol. 21, no. 16, p. 5397, Aug. 2021, doi: 10.3390/s21165397.

[14] K. Mascher, M. Watzko, A. Koppert, J. Eder, P. Hofer, and M. Wieser, 'NIKE BLUETRACK: Blue Force Tracking in GNSS-Denied Environments Based on the Fusion of UWB, IMUs and 3D Models', *Sensors*, vol. 22, no. 8, p. 2982, Apr. 2022, doi: 10.3390/s22082982.

[15] C. Günther, 'A Survey of Spoofing and Counter-Measures: A Survey of Spoofing and Counter-Measures', *J Inst Navig*, vol. 61, no. 3, pp. 159–177, Sep. 2014, doi: 10.1002/navi.65.

[16] D. Schmidt, K. Radke, S. Camtepe, E. Foo, and M. Ren, 'A Survey and Analysis of the GNSS Spoofing Threat and Countermeasures', *ACM Comput. Surv.*, vol. 48, no. 4, pp. 1–31, May 2016, doi: 10.1145/2897166.

[17] W. Liu, Z. Li, S. Sun, M. K. Gupta, H. Du, R. Malekian, M. A. Sotelo, and W. Li, 'Design a Novel Target to Improve Positioning Accuracy of Autonomous Vehicular Navigation System in GPS Denied Environments', *IEEE Trans. Ind. Inf.*, vol. 17, no. 11, pp. 7575–7588, Nov. 2021, doi: 10.1109/TII.2021.3052529.

[18] C. I. Rablau, 'Lidar: a new self-driving vehicle for introducing optics to broader engineering and non-engineering audiences', in *Fifteenth Conference on Education and Training in Optics and Photonics: ETOP 2019*, A.-S. Poulin-Girard and J. A. Shaw, Eds., Quebec City, Canada: SPIE, Jul. 2019, p. 138. doi: 10.1117/12.2523863.

[19] C. Zhang, Z. Huang, M. H. Ang, and D. Rus, 'LiDAR Degradation Quantification for Autonomous Driving in Rain', in *2021 IEEE/RSJ International Conference on Intelligent Robots and Systems (IROS)*, Sep. 2021, pp. 3458–3464. doi: 10.1109/IROS51168.2021.9636694.

[20] J. Vargas Rivero, T. Gerbich, B. Buschardt, and J. Chen, 'The Effect of Spray Water on an Automotive LIDAR Sensor: A Real-Time Simulation Study', *IEEE Trans. Intell. Veh.*, vol. 7, no. 1, pp. 57–72, Mar. 2022, doi: 10.1109/TIV.2021.3067892.

[21] G. Cheng, Z. Wang, and J. Y. Zheng, 'Modeling Weather and Illuminations in Driving Views Based on Big-Video Mining', *IEEE Trans. Intell. Veh.*, vol. 3, no. 4, pp. 522–533, Dec. 2018, doi: 10.1109/TIV.2018.2873920.

[22] S.-H. Lee and C. C. Chung, 'Robust Multirate On-Road Vehicle Localization for Autonomous Highway Driving Vehicles', *IEEE Trans. Contr. Syst. Technol.*, vol. 25, no. 2, pp. 577–589, Mar. 2017, doi: 10.1109/TCST.2016.2562607.

[23] M. Brossard, A. Barrau, and S. Bonnabel, 'AI-IMU Dead-Reckoning', *IEEE Trans. Intell. Veh.*, vol. 5, no. 4, pp. 585–595, Dec. 2020, doi: 10.1109/TIV.2020.2980758.

[24] G. De Pasquale and A. Somà, 'Reliability Testing Procedure for MEMS IMUs Applied to Vibrating Environments', *Sensors*, vol. 10, no. 1, pp. 456–474, Jan. 2010, doi: 10.3390/s100100456.

[25] T. Trippel, O. Weisse, W. Xu, P. Honeyman, and K. Fu, 'WALNUT: Waging Doubt on the Integrity of MEMS Accelerometers with Acoustic Injection Attacks', in *2017 IEEE European Symposium on Security and Privacy (EuroS&P)*, Paris: IEEE, Apr. 2017, pp. 3–18. doi: 10.1109/EuroSP.2017.42.

[26] National Transportation Safety Committee (NTSC), *Aircraft Accident Investigation Report Boeing 737–4Q8 PK–KKW*. Ministry of Transportation Republic of Indonesia, 2008.

[27] K. Eckenhoff, P. Geneva, and G. Huang, 'Sensor-Failure-Resilient Multi-IMU Visual-Inertial Navigation', in *2019 International Conference on Robotics and Automation (ICRA)*, Montreal, QC, Canada: IEEE, May 2019, pp. 3542–3548. doi: 10.1109/ICRA.2019.8794295.

[28] Z. Zhao, J. Wang, J. Cao, W. Gao, and Q. Ren, 'A Fault-tolerant Architecture for Mobile Robot Localization', in *2019 IEEE 15th International Conference on Control and Automation (ICCA)*, Edinburgh, United Kingdom: IEEE, Jul. 2019, pp. 584–589. doi: 10.1109/ICCA.2019.8899574.

[29] J. Liu and G. Guo, 'Vehicle Localization During GPS Outages With Extended Kalman Filter and Deep Learning', *IEEE Trans. Instrum. Meas.*, vol. 70, pp. 1–10, 2021, doi: 10.1109/TIM.2021.3097401.

[30] SAE Publications, 'Vehicle dynamics terminology', *SAE International*, vol. No. J670, 2008.

[31] P. Crocoll, L. Görcke, G. F. Trommer, and F. Holzapfel, 'Unified Model Technique for Inertial Navigation Aided by Vehicle Dynamics Model: Unified Model Technique for Model-Aided Navigation', *J Inst Navig*, vol. 60, no. 3, pp. 179–193, Sep. 2013, doi: 10.1002/navi.39.

[32] A. Lima, A. Welte, P. Bonnifait, and P. Xu, 'LiDAR Observations by Motion Compensation and Scan Accumulation', in *2020 16th International Conference on Control, Automation, Robotics and Vision (ICARCV)*, Shenzhen, China: IEEE, Dec. 2020, pp. 400–405. doi: 10.1109/ICARCV50220.2020.9305365.

[33] R. C. Dorf and R. H. Bishop, *Modern control systems*, Thirteenth edition. Hoboken: Pearson, 2016.

[34] M. Khaghani and J. Skaloud, 'Autonomous Vehicle Dynamic Model-Based Navigation for Small UAVs: Autonomous VDM Based Navigation for Small UAVs', *J Inst Navig*, vol. 63, no. 3, pp. 345–358, Sep. 2016, doi: 10.1002/navi.140.

[35] C. Chen, D. Xing, K. Cao, and B. Zhang, 'Research on unmanned vehicle control algorithm during driving curve', in *2016 35th Chinese Control Conference (CCC)*, Chengdu: IEEE, Jul. 2016, pp. 8836–8841. doi: 10.1109/ChiCC.2016.7554769.

[36] L. Ljung, 'Perspectives on system identification', *Annual Reviews in Control*, vol. 34, no. 1, pp. 1–12, Apr. 2010, doi: 10.1016/j.arcontrol.2009.12.001.

[37] R. Rajamani, *Vehicle Dynamics and Control*. in Mechanical Engineering Series. Boston, MA: Springer US, 2012. doi: 10.1007/978-1-4614-1433-9.

[38] L. Ljung, *System identification: theory for the user*, 2nd ed. in Prentice Hall information and system sciences series. Upper Saddle River, NJ: Prentice Hall PTR, 1999.

[39] F. Daum, 'Nonlinear filters: beyond the Kalman filter', *IEEE Aerosp. Electron. Syst. Mag.*, vol. 20, no. 8, pp. 57–69, Aug. 2005, doi: 10.1109/MAES.2005.1499276.

[40] R. E. Kalman, 'A New Approach to Linear Filtering and Prediction Problems', *Journal of Basic Engineering*, vol. 82, no. 1, pp. 35–45, Mar. 1960, doi: 10.1115/1.3662552.

[41] F. Dellaert and M. Kaess, 'Factor Graphs for Robot Perception', *FNT in Robotics*, vol. 6, no. 1–2, pp. 1–139, 2017, doi: 10.1561/2300000043.

[42] Mohamed Belrzaeg, Abdussalam Ali Ahmed, Amhimmid Q Almabrouk, Mohamed Mohamed Khaleel, Alforjani Ali Ahmed, and Meshaal Almukhtar, 'Vehicle dynamics and tire models: An overview', *World J. Adv. Res. Rev.*, vol. 12, no. 1, pp. 331–348, Oct. 2021, doi: 10.30574/wjarr.2021.12.1.0524.

[43] Kiam Heong Ang, G. Chong, and Yun Li, 'PID control system analysis, design, and technology', *IEEE Trans. Contr. Syst. Technol.*, vol. 13, no. 4, pp. 559–576, Jul. 2005, doi: 10.1109/TCST.2005.847331.

[44] E. H. Dursun and A. Durdu, 'Speed Control of a DC Motor with Variable Load Using Sliding Mode Control', *IJCEE*, vol. 8, no. 3, pp. 219–226, 2016, doi: 10.17706/IJCEE.2016.8.3.219-226.

[45] L. Ljung, 'Identification for control: simple process models', in *Proceedings of the 41st IEEE Conference on Decision and Control, 2002.*, Las Vegas, NV, USA: IEEE, 2002, pp. 4652–4657. doi: 10.1109/CDC.2002.1185112.

[46] T. Liu, Q.-G. Wang, and H.-P. Huang, 'A tutorial review on process identification from step or relay feedback test', *Journal of Process Control*, vol. 23, no. 10, pp. 1597–1623, Nov. 2013, doi: 10.1016/j.jprocont.2013.08.003.

[47] J. Gurland and P. Whittle, 'Hypothesis Testing in Time Series Analysis', *Journal of the American Statistical Association*, vol. 49, no. 265, p. 197, Mar. 1954, doi: 10.2307/2281054.

[48] H. Akaike, 'A new look at the statistical model identification', *IEEE Trans. Automat. Contr.*, vol. 19, no. 6, pp. 716–723, Dec. 1974, doi: 10.1109/TAC.1974.1100705.

[49] N. S. Nise, *Control systems engineering*, Seventh edition. Hoboken, NJ: Wiley, 2015.

[50] E. Takeuchi and T. Tsubouchi, 'A 3-D Scan Matching using Improved 3-D Normal Distributions Transform for Mobile Robotic Mapping', in *2006 IEEE/RSJ International Conference on Intelligent Robots and Systems*, Beijing, China: IEEE, Oct. 2006, pp. 3068–3073. doi: 10.1109/IROS.2006.282246.

[51] N. Koenig and A. Howard, 'Design and use paradigms for gazebo, an open-source multi-robot simulator', in *2004 IEEE/RSJ International Conference on Intelligent Robots and Systems (IROS) (IEEE Cat. No.04CH37566)*, Sendai, Japan: IEEE, 2004, pp. 2149–2154. doi: 10.1109/IROS.2004.1389727.

[52] L. Crosato, H. P. H. Shum, E. S. L. Ho, and C. Wei, 'Interaction-aware Decision-making for Automated Vehicles using Social Value Orientation', *IEEE Trans. Intell. Veh.*, pp. 1–11, 2022, doi: 10.1109/TIV.2022.3189836.

[53] K. Viana, A. Zubizarreta, and M. Diez, 'A Reconfigurable Framework for Vehicle Localization in Urban Areas', *Sensors*, vol. 22, no. 7, p. 2595, Mar. 2022, doi: 10.3390/s22072595.

[54] A. Dosovitskiy, G. Ros, F. Codevilla, A. Lopez, and V. Koltun, 'CARLA: An Open Urban Driving Simulator', in *the 1st Annual Conference on Robot Learning*, 2017, pp. 1–16.

[55] P. Hart, N. Nilsson, and B. Raphael, 'A Formal Basis for the Heuristic Determination of Minimum Cost Paths', *IEEE Trans. Syst. Sci. Cyber.*, vol. 4, no. 2, pp. 100–107, 1968, doi: 10.1109/TSSC.1968.300136.

[56] R. C. Conlter, 'Implementation of the Pure Pursuit Path Tracking Algorithm', Carnegie-Mellon UNIV Pittsburgh PA Robotics INST, 1992.

[57] B. Mashadi and D. Crolla, *Vehicle powertrain systems*, 1st ed. Chichester, West Sussex, U.K: Wiley, 2012.

[58] M. Harrer and P. Pfeffer, Eds., *Steering Handbook*. Cham: Springer International Publishing, 2017. doi: 10.1007/978-3-319-05449-0.

[59] M. Magnusson, *The Three-Dimensional Normal-Distributions Transform an Efficient Representation for Registration, Surface Analysis, and Loop Detection*. Örebro: Örebro universitet, 2009.

Penggao Yan received the bachelor's degree in Communication Engineering in 2018 and the master's degree in Pattern Recognition and Intelligent Systems in 2021, both from Wuhan University, China. He is currently pursuing a Ph.D. degree at the Department of Aeronautical and Aviation Engineering, the Hong Kong Polytechnic University.

His research interests include autonomous vehicles, control aided localization, sensor fusion, fault detection in localization systems.

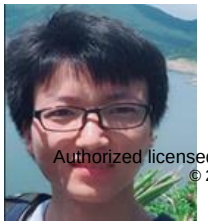

Weisong Wen (Member, IEEE) received a Ph.D. degree in mechanical engineering, the Hong Kong Polytechnic University. He was a visiting student researcher at the University of California, Berkeley (UCB) in 2018. He is currently a research assistant professor in the Department of Aeronautical and Aviation Engineering, the Hong Kong Polytechnic University.

His research interests include multi-sensor integrated localization for autonomous vehicles, SLAM, and GNSS positioning in urban canyons.

Li-Ta Hsu (Senior Member, IEEE) received the B.S. and Ph.D. degrees in aeronautics and astronautics from National Cheng Kung University, Tainan City, Taiwan, in 2007 and 2013, respectively. He is currently an Associate Professor with the Department of Aeronautical and Aviation Engineering, The Hong Kong Polytechnic University. He is also Limin Endowed Young Scholar in Aerospace Navigation. He was a Visiting Researcher with the Faculty of Engineering, University College London, London, U.K., and the Tokyo University of Marine Science and Technology, Tokyo, Japan, in 2012 and 2013, respectively. Dr. Hsu was selected as a Japan Society for the Promotion of Sciences Postdoctoral Fellow with the Institute of Industrial Science, University of Tokyo, Tokyo, Japan, and worked from 2014 to 2016. He is an Associate Fellow with the Royal Institute of Navigation, London, U.K. He is currently a member of ION and and a member of the editorial board and reviewer in professional journals related to GNSS. In 2013, he won a Student Paper Award and two Best Presentation Awards from the Institute of Navigation (ION).

His research interests include GNSS positioning in challenging environments and localization for pedestrian, autonomous driving vehicle, and unmanned aerial vehicle.